

Physical properties and magnetic structure of a layered antiferromagnet $PrPd_{0.82}Bi_2$

Meng Yang(杨萌), Changjiang Yi(伊长江), Fengfeng Zhu(朱锋锋), Xiao Wang(王霄), Dayu Yan(闫大禹), Shanshan Miao(苗杉杉), Yixi Su(苏夷希), Youguo Shi(石友国)

Citation: Chin. Phys. B . 2020, 29(6): 067502 . **doi:** 10.1088/1674-1056/ab889f
Journal homepage: http://cpb.iphy.ac.cn; http://iopscience.iop.org/cpb

What follows is a list of articles you may be interested in

Temperature-dependent interlayer exchange coupling strength in synthetic antiferromagnetic$[Pt/Co]_2/Ru/[Co/Pt]_4$ multilayers

Yong Li(李勇), Xiangjun Jin(金香君), Pengfei Pan(潘鹏飞), Fu Nan Tan, Wen Siang Lew, Fusheng Ma(马付胜)

Chin. Phys. B . 2018, 27(12): 127502 . **doi:** 10.1088/1674-1056/27/12/127502

Mn-based permanent magnets

Jinbo Yang(杨金波), Wenyun Yang(杨文云), Zhuyin Shao(邵珠印), Dong Liang(梁栋), Hui Zhao(赵辉), Yuanhua Xia(夏元华), Yunbo Yang(杨云波)

Chin. Phys. B . 2018, 27(11): 117503 . **doi:** 10.1088/1674-1056/27/11/117503

The magnetic properties and magnetocaloric effects in binary *R*-*T* (*R*=Pr, Gd, Tb, Dy, Ho, Er, Tm; *T*=Ga, Ni, Co, Cu) intermetallic compounds

Xin-Qi Zheng(郑新奇), Bao-Gen Shen(沈保根)

Chin. Phys. B . 2017, 26(2): 027501 . **doi:** 10.1088/1674-1056/26/2/027501

Growth and characterization of $CaCu_3Ru_4O_{12}$ single crystal

Wang Rong-Juan, Zhu Yuan-Yuan, Wang Li, Liu Yong, Shi Jing, Xiong Rui, Wang Jun-Feng

Chin. Phys. B . 2015, 24(9): 097501 . **doi:** 10.1088/1674-1056/24/9/097501

High sum-frequency generation in dielectric/antiferromagnet/Ag sandwich structures

Fu Shu-Fang, Liang Hong, Zhou Sheng, Wang Xuan-Zhang

Chin. Phys. B . 2014, 23(5): 057503 . **doi:** 10.1088/1674-1056/23/5/057503

Physical properties and magnetic structure of a layered antiferromagnet $PrPd_{0.82}Bi_2$*

Meng Yang(杨萌)[1,2], Changjiang Yi(伊长江)[1], Fengfeng Zhu(朱锋锋)[3], Xiao Wang(王霄)[3], Dayu Yan(闫大禹)[1,2], Shanshan Miao(苗杉杉)[1], Yixi Su(苏夷希)[3,†], and Youguo Shi(石友国)[1,2,‡]

[1] *Beijing National Laboratory for Condensed Physics and Institute of Physics, Chinese Academy of Sciences, Beijing* 100190, *China*
[2] *Center of Materials Science and Optoelectronics Engineering, University of Chinese Academy of Sciences, Beijing* 100049, *China*
[3] *Jülich Centre for Neutron Science (JCNS) at Heinz Maier-Leibnitz Zentrum (MLZ), Forschungszentrum Jülich GmbH, Lichtenbergstraße* 1, 85748 *Garching, Germany*

(Received 5 March 2019; revised manuscript received 3 April 2020; accepted manuscript online 13 April 2020)

We report the physical properties, crystalline and magnetic structures of singe crystals of a new layered antiferromagnetic (AFM) material $PrPd_{0.82}Bi_2$. The measurements of magnetic properties and heat capacity indicate an AFM phase transition at $T_N \sim 7$ K. A large Sommerfeld coefficient of 329.23 mJ·mol^{-1}·K^{-2} is estimated based on the heat capacity data, implying a possible heavy-fermion behavior. The magnetic structure of this compound is investigated by a combined study of neutron powder and single-crystal diffraction. It is found that an A-type AFM structure with magnetic propagation wavevector $\boldsymbol{k} = (0\ 0\ 0)$ is formed below T_N. The Pr^{3+} magnetic moment is aligned along the crystallographic c-axis with an ordered moment of 1.694(3) μ_B at 4 K, which is smaller than the effective moment of the free Pr^{3+} ion of 3.58 μ_B. $PrPd_{0.82}Bi_2$ can be grown as large as 1 mm×1 cm in area with a layered shape, and is very easy to be cleaved, providing a unique opportunity to study the interplay between magnetism, possible heavy fermions, and superconductivity.

Keywords: correlated electronic system, layered antiferromagnet, neutron scattering, magnetic structure

PACS: 75.30.Mb, 75.50.Ee, 25.40.Dn, 28.20.Cz **DOI:** 10.1088/1674-1056/ab889f

1. Introduction

The layered pnictide materials such as iron-based superconductors have attracted much attention in the condensed matter physics community.[1–6] As an extensively investigated large family of materials with the general chemical formula of $AMPn_2$ (A = alkali earth or rare earth element, M = transition metal, and Pn = pnictogen), this series of compounds are usually found to have a tetragonal $ZrCuSi_2$-type structure (space group $P4/nmm$), where the A, MPn, and Pn layers are alternately stacked with each other. Emergent physical properties, such as superconductivity in $LaNi_{1-x}Bi_2$, $LaPd_{0.85}Bi_2$, and doped $CaFeAs_2$,[7–11] and possible Dirac fermions in the topological semimetals $SrMnBi_2$, $BaMnBi_2$, and $BaMnSb_2$[12–14] have been discovered recently. Replacing alkali earth elements or lanthanum with magnetic rare earth elements, such as Ce–Nd, Eu, Yb *et al.*, may introduce additional ingredients to these materials, such as antiferromagnetic (AFM) order, Kondo effect, and heavy-fermion behavior. For example, the Kondo effect has been observed in some Ce-based intermetallic compounds,[15–18] due to the partial screening of the local magnetic moments of the 4f electrons at low temperatures. At much lower temperature, the AFM order may appear because of the dominating Ruderman–Kittel–Kasuya–Yosida (RKKY) interaction that would favor an antiferromagnetic coupling between the local moments of the 4f electrons, such as in $PrPdSb_2$ ($T_N \sim 7.6$ K),[19] $CePd_{1-x}Bi_2$ ($T_N \sim 6$ K),[18] $LnAuBi_2$ ($T_N \sim 2.6$ K for Ln = Nd; $T_N \sim 7.4$ K for Ln = Pr, *et al.*[20]), and $ErNi_{1-x}Sb_2$ ($T_N \sim 3.5$ K).[21] However, the bulk superconductivity observed in the polycrystalline $CeNi_{1-x}Bi_2$[22] is still controversial. Recent report based on the studies of a series of $LnNi_{1-x}Bi_2$ (Ln = Ce–Nd, Sm, Gd–Dy) single crystals has suggested that the observed superconductivity is not an intrinsic phenomenon but is likely resulted from minority phases.[23]

In this paper, we report the physical properties and magnetic structure of a new member of the $AMPn_2$ family, $PrPd_{1-x}Bi_2$. Similar to previously reported isostructural materials containing the Ni or Pd element, $PrPd_{1-x}Bi_2$ also possesses Pd vacancies, and the value of x is estimated to be 0.82 based on the single-crystal x-ray diffraction (XRD) analysis. We found that $PrPd_{0.82}Bi_2$ exhibits an AFM order below ~ 7 K, and neutron diffraction experiments reveal an A-type AFM structure with the magnetic moments of the Pr^{3+} ions aligned along the crystallographic c-axis. A large Sommerfeld coefficient estimated from heat capacity implies a possible heavy-fermion behavior. Moreover, given the absence of

*Project supported by the National Key Research and Development Program of China (Grant Nos. 2017YFA0302901 and 2016YFA0300604), the National Natural Science Foundation of China (Grant No. 11774399), Beijing Natural Science Foundation, China (Grant No. Z180008), the K. C. Wong Education Foundation (Grant No. GJTD-2018-01), the DAAD-PPP programme, and the joint German-Sino HGF-OCPC Postdoc Programme.

†Corresponding author. E-mail: y.su@fz-juelich.de
‡Corresponding author. E-mail: ygshi@iphy.ac.cn

© 2020 Chinese Physical Society and IOP Publishing Ltd

diamagnetism in the sample, we argue that the observed zero-resistivity in $PrPd_{0.82}Bi_2$ is possibly caused by the minority phases. Thus, we suggest that $PrPd_{0.82}Bi_2$ may provide an opportunity to clarify the existing controversies about the low temperature physical properties of this class of materials.

2. Experimental details

Single crystals of $PrPd_{0.82}Bi_2$ were grown by the Bi-flux method. High-purity Pr, Pd, and Bi elements were put in an alumina crucible with a molar ratio of 1 : 1 : 10. The operations were performed in a glove box filled with argon. Then the crucible was sealed in a quartz tube under high vacuum followed by heating to 1273 K, dwelling for 5 hours, and slowly cooling down to 873 K. Afterward, excess Bi flux was removed in a centrifuge. Large and plate-like single crystals with metallic luster were obtained with a typical size of 4 mm×9 mm×1 mm. The crystals are sensitive to the damp air and will be pleated and turning yellow after air-exposure for several hours.

Single-crystal XRD was carried out by using a Bruker D8 Venture diffractometer equipped with Mo $K\alpha$ radiation ($\lambda = 0.71073$ Å). The collected data was refined by full-matrix least-squares fitting on F^2 using the SHELXL-2016/6 program. Powder XRD was performed on a Bruker D2 Phaser powder diffractometer by using Cu $K\alpha$ radiation. The powder samples were obtained from grinding some single crystals. All of the XRD data were collected at room temperature. Chemical composition of the single crystals was analyzed by energy-dispersive x-ray spectroscopy (EDX) in a Hitachi S-4800 at an accelerating voltage of 15 kV.

Magnetic susceptibility (χ) was measured in a magnetic properties measurement system (MPMS, Quantum Design Inc.) between 2 K and 300 K at various fixed applied magnetic fields in field-cooling (FC) and zero-field-cooling (ZFC) configurations. Isothermal magnetization (M–H) was measured in a sweeping field from −70 kOe to 70 kOe. Both applied field directions perpendicular and parallel to the crystallographic c-axis were measured. The C_p and electronic resistivity ρ were measured from 2 K to 300 K in various fixed magnetic fields by a physical property measurement system (PPMS, Quantum Design Inc.). The C_p was measured by using a thermal-relaxation method and the ρ was measured via four-probe technique with dc mode.

Neutron scattering experiments were carried out at the polarized neutron instrument DNS at Heinz Maier-Leibnitz Zentrum (MLZ) at Garching, Germany. To determine the magnetic structure of $PrPd_{0.82}Bi_2$, one piece of single crystal weighing ∼ 200 mg was fixed on an aluminum sample stick in a standard top-loading 4 K closed-cycle cryostat, with the (H 0 L) reciprocal plane being placed in the horizontal scattering plane. The wavelength of the neutron beam used for the measurements is $\lambda = 4.2$ Å. The polarization rate of the neutron beam is about ∼ 96%. The polarized neutron diffraction intensities were measured in the X non-spin-flip (Xnsf), X spin-flip (Xsf), Z non-spin-flip (Znsf), and Z spin-flip (Zsf) scattering channels, respectively. The X polarization is defined as along the Q direction, i.e., the momentum transfer direction in the horizontal scattering plane, and the Z polarization is perpendicular to the scattering plane. The standard procedure for the flipping ratio correction was employed for the data treatment. Complementary non-polarized neutron powder diffraction (NPD) experiment was also performed on a grounded $PrPd_{0.82}Bi_2$ powder sample at DNS. The powders were placed in a thin-walled aluminum sample can. The data was collected at $T = 12$ K and 4 K, which were above and below the AFM phase transition temperature, respectively. Both powder and single-crystal magnetic structure refinements were performed with the FullProf software package.

3. Results and discussion

3.1. Crystalline structure

Single-crystal XRD refinements indicate that $PrPd_{0.82}Bi_2$ crystallizes in a $ZrCuSi_2$-type tetragonal structure with space group $P/4nmm$. The refined lattice parameters are $a = b = 4.626(2)$ Å, and $c = 9.610(5)$ Å. More detailed information about the refinement and the structural parameters is summarized in Tables 1 and 2. Results from single-crystal refinement show that the Pd atom positions are not fully occupied but with a vacancy rate of $x \sim 0.18$, which is common in the 112-type materials. The normalized XRD intensity of the (0 0 L) reflections is shown in Fig. 1(a). The high quality of the single crystals can be inferred from the observed sharp peaks. The inset (i) in Fig. 1(a) shows the schematic crystal structure with a stacking of –Bi/Pr/BiPd/Pr– layers along the c-axis. In this layered structure, the BiPd-layer is in analogy to the FeAs-layer in the iron-based superconductors. The Bi atoms form a square net lattice where the two-dimensional Dirac or Weyl fermions are usually expected to be located.[12,14,24–28] A picture shown in the inset (ii) in Fig. 1(a) shows the layered nature and typical size of the $PrPd_{0.82}Bi_2$ single crystals.

Figure 1(b) shows the refined XRD pattern of the powder sample that is grounded from a small crystal via the Rietveld method. The preferred orientation is included in the refinement. The observed data can be well refined, yielding $R_p = 5.23\%$, $R_{wp} = 6.65\%$, and $\chi^2 = 1.21$. The obtained structural parameters are consistent to those obtained with the single-crystal XRD refinement. Meanwhile, no impurity phases were observed. Therefore, this structure was also adopted to refine the non-polarized NPD data that will be discussed later.

Table 1. Crystallographic and structure refinement data for $PrPd_{0.82}Bi_2$.

Empirical formula	$PrPd_{0.82(4)}Bi_2$
Formula weight/g·mol^{-1}	523.036
Temperature	273(2) K
Wavelength	Mo $K\alpha$ (0.71073 Å)
Crystal system	tetragonal
Space group	$P4/nmm$ (129)
Unit cell dimensions/Å	$a = b = 4.626(2)$, $c = 9.610(5)$
Cell volume/Å^3	205.6(2)
Z	2
Density, calculated/g·cm^{-3}	10.43
$h\ k\ l$ range	$-5 \le h \le 6$, $4 \le k \le 6$, $12 \le l \le 12$
$2\theta_{min}/(^\circ)$	8.482
$2\theta_{max}/(^\circ)$	56.826
Linear absorption coeff./mm^{-1}	100.232
Absorption correction	multi-scan
No. of reflections	1152
T_{min}/T_{max}	0.003/0.03
No. independent reflections	182
No. observed reflections	173[$I > 2\sigma(I)$]
$F(0\,0\,0)$	525
R indexes	6.79% ($R_1[F_o > 4\sigma(F_o)]$), 17.9% (wR_2)
Weighting scheme	$w = 1/[\sigma^2(F_o^2) + (0.0897P)^2 + 28.6161P]$, where $P = [\mathrm{Max}(F_o^2) + 2F_c^2]/3$
Refinement software	SHELXL-2016/6

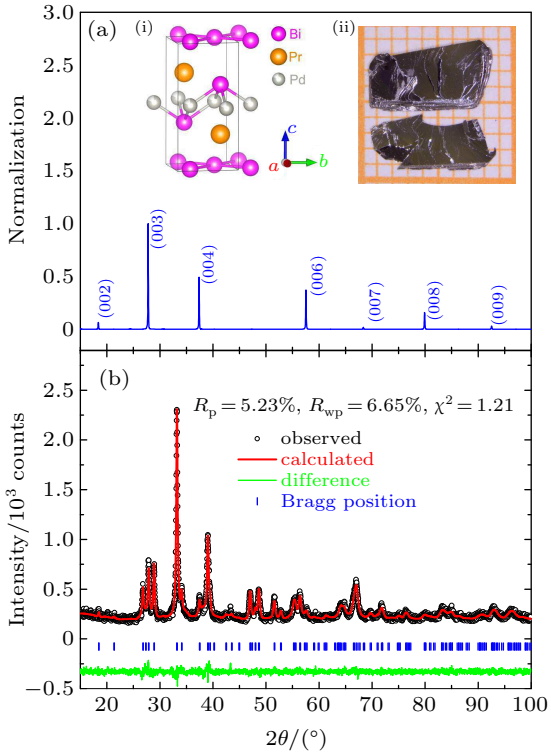


Fig. 1. (a) Diffraction pattern of a series of (0 0 L) reflections of a freshly cleaved $PrPd_{0.82}Bi_2$ single crystal. Inset shows (i) the schematic structure and (ii) a picture of typical single crystals. (b) Refined powder XRD pattern of a $PrPd_{0.82}Bi_2$ powder sample that is grounded from a small crystal.

The chemical composition of some selected crystals was determined by EDX to be Pr : Pd : Bi = 25.96 : 23.29 : 50.74. The Pd vacancy found by EDX (~ 0.92) was slightly larger than the value (~ 0.82) that was refined by single-crystal XRD. Similar vacancies were also reported in the isostructural materials $LaPd_{1-x}Bi_2$ and $CePd_{1-x}Bi_2$.[8,9,18]

Table 2. Atomic coordinates and equivalent isotropic thermal parameters of $PrPd_{0.82}Bi_2$.

Atoms	WP[a]	x	y	z	U_{eq}/Å^2 [b]	OP[c]
Bi01	2c	3/4	3/4	0.6606(3)	0.0287(9)	1
Bi02	2a	1/4	−1/4	0	0.0262(8)	1
Pr	2c	3/4	−1/4	0.2699(4)	0.0252(10)	1
Pd	2b	3/4	1/4	0	0.0280(16)	0.82(4)

[a]Wyckoff positions; [b]equivalent isotropic thermal parameter; [c]occupation.

3.2. Magnetic properties

Magnetic properties were measured on a typical single crystal of $PrPd_{0.82}Bi_2$. Data collected in both ZFC and FC configurations are almost identical with each other. Figure 2(a) shows the temperature and field-direction dependence of χ in various fixed applied fields. A paramagnetic to AFM phase transition with $T_N \sim 7$ K is observed when cooling down the sample. As increasing the strength of the applied field, the AFM peak shifts to the lower temperature in both the applied field being parallel and perpendicular to the c-axis. A plateau appears at around $T = 4$ K indicating that the magnetic moments in $PrPd_{0.82}Bi_2$ are suppressed and shall be saturated if a higher field is applied. The magnetic susceptibility around T_N for $H \parallel c$ (~ 0.15 emu·mol^{-1}) is almost twice larger than that for $H \perp c$ (~ 0.08 emu·mol^{-1}). This anisotropic magnetic behavior suggests that the magnetic easy axis is aligned along the c-axis, which is confirmed by neutron scattering experiments that will be discussed latter. Under low magnetic field, $PrPd_{0.82}Bi_2$ shows a weak diamagnetic jump at $T \sim 2.5$ K, as shown in Fig. S1 in the supplementary information, which may be caused by the superconducting behavior that was also inferred in the resistivity measurement.

The inverse magnetic susceptibility χ^{-1} versus T is plotted for a fixed applied field $H = 10$ kOe, as shown in Fig. 2(b). The Curie–Weiss law, with a formula of $\chi = C/(T - T_\theta)$, where C is the Curie constant and T_θ is the Weiss temperature, was used to fit data above 120 K. The effective magnetic moment is roughly determined by $\mu_{eff} = \sqrt{8C}$, yielding $\mu_{eff} = 3.86\ \mu_B$ for $H \parallel c$ and $\mu_{eff} = 3.92\ \mu_B$ for $H \perp c$, respectively. The estimated magnetic moments are in good accordance with the theoretical value of 3.58 μ_B for the free Pr^{3+} ions. Isothermal magnetization is shown in the inset of Fig. 2(b), which is measured for $H \parallel c$ and $H \perp c$ at 2 K and 300 K, respectively. A spin-flop phase transition is observed at $T = 2$ K with an onset field $H \sim 30$ kOe. This anisotropic magnetization is often seen in the layered materials such as tetragonal $EuMnPn_2$ and hexagonal $EuCd_2Pn_2$ (Pn = pnictogen)[25,29,30] and the related compounds. In these systems, the magnetic moments of the rare earth elements are found commonly aligned along the c-axis, usually accompanied with a spin-flop transition at low temperatures in applied fields.

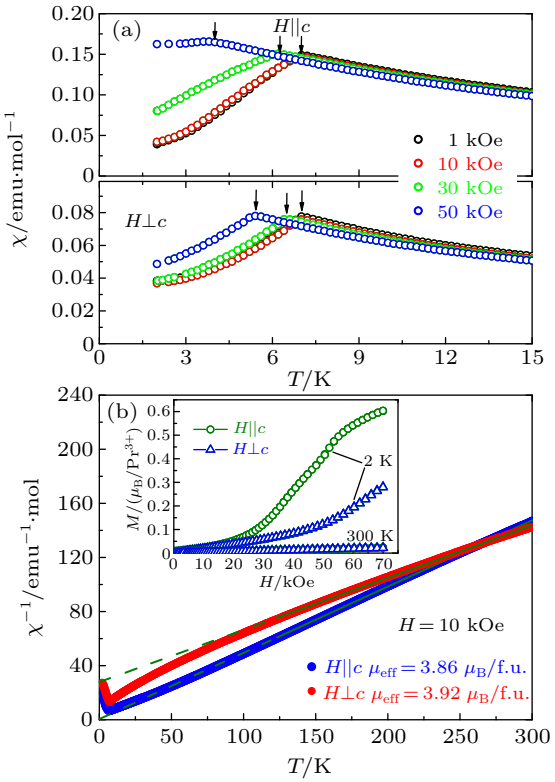


Fig. 2. (a) Temperature and magnetic fields dependence of $PrPd_{0.82}Bi_2$ single crystal, which is measured with the applied field being parallel and perpendicular to the c-axis. (b) Temperature dependence in a fixed field of 10 kOe. Green dash line represents the Curie–Weiss fitting. The inset shows isothermal magnetization measured with the applied field parallel and perpendicular to the c-axis at various temperatures.

3.3. Heat capacity

The C_p versus T without applied field is plotted in Fig. 3(a). The sharp anomaly at low temperature indicates an AFM phase transition that is also visible in magnetic susceptibility. For a more quantitative analysis, the Debye–Einstein model was utilized to estimate the electronic and phononic contributions by the following formula:[29]

$$C_{\text{el+ph}} = \gamma_0 T + \alpha 9nR\left(\frac{T}{\theta_{\text{D}}}\right)^3 \int_0^{\theta_{\text{D}}/T} \frac{x^4 \mathrm{e}^x}{(\mathrm{e}^x - 1)^2}\mathrm{d}x + (1-\alpha)\,3nR\frac{(\theta_{\text{E}}/T)^2\,\mathrm{e}^{\theta_{\text{E}}/T}}{\left(\mathrm{e}^{\theta_{\text{E}}/T} - 1\right)^2},$$

where γ_0 is the heat coefficient of the background conduction electrons, θ_{D} and θ_{E} are respectively the Debye and Einstein temperatures, and α is the contribution ratio of these two components. The data above $T = 16$ K was fitted and yielded that $\gamma_0 = 5.8$ mJ·mol^{-1}·K^{-2}, $\theta_{\text{D}} = 201.95$ K, and $\theta_{\text{E}} = 66.18$ K. By using these refined parameters, the fitting was extended to 2 K, and the fitting result was taken as the estimated non-magnetic contributions for further analysis. The inset of Fig. 3(a) shows the C_p/T vs. T^2 curve at low temperature, which can be well described by the following formula:

$$C_p/T = \gamma + \beta T^2.$$

This gives out the value of the Sommerfeld coefficient $\gamma = 329.23$ mJ·mol^{-1}·K^{-2}, which is almost two orders of magnitude larger than that of the background conduction electrons with $\gamma_0 = 5.8$ mJ·mol^{-1}·K^{-2}. This clearly shows that the effective mass of the charge carriers is somehow enhanced. To clearly verify the magnetic field dependence of the AFM order, the C_p/T vs. T plot was measured in various magnetic fields and plotted in Fig. 3(b). During the measurements, the magnetic field parallel to the c-axis was applied. The AFM peak shifts to lower temperature, and is eventually suppressed with increasing magnetic field. This is consistent with the common behavior of an AFM order.

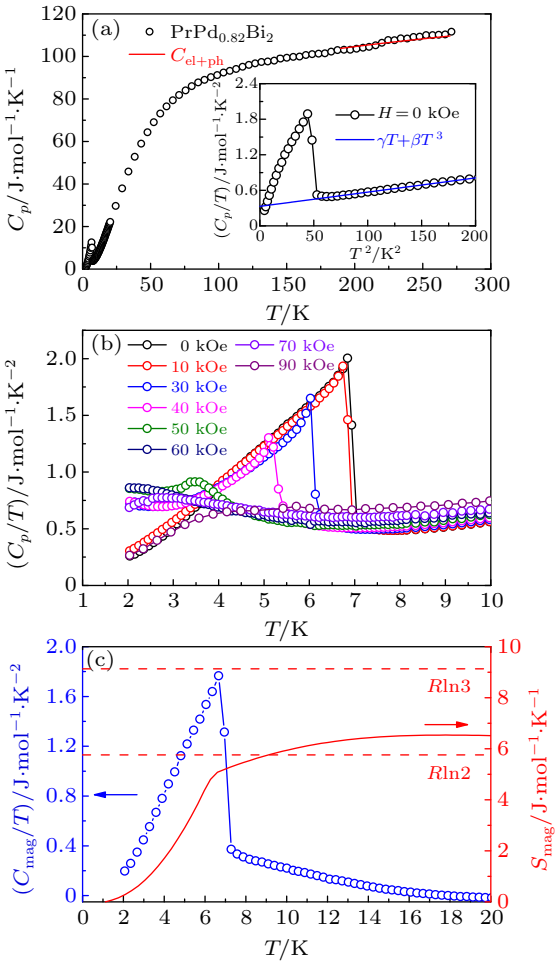


Fig. 3. (a) Temperature dependent specific heat capacity without magnetic field. Black circles are observed C_p and red continuous line is the fit of electron and lattice contributions by Debye and Einstein models. The inset: C_p/T vs. T^2 plots without magnetic field below $T^2 = 200$ K^2 with a linear fit. (b) C_p/T vs. T curves in various fixed applied fields from 0 kOe to 90 kOe. (c) Magnetic specific heat capacity C_{mag}/T (blue circles) and entropy S_{mag} (solid red line) as functions of temperature.

Figure 3(c) displays the magnetic heat capacity (C_{mag}/T) and magnetic entropy (S_{mag}) as a function of temperature. The S_{mag} is estimated by integrating the C_{mag}/T vs. T curve below $T = 20$ K after subtracting the non-magnetic background that is estimated by the Debye–Einstein model, indicating that the remaining entropy contributions are almost entirely from the

magnetic phase transition. The $\Delta S_{\rm mag}$ is roughly estimated to be 6.51 J·mol^{-1}·K^{-1}, which is smaller than Rln3 but slightly larger than Rln2, implying that the ground state of the Pr f-electrons may be greatly influenced by the crystalline electronic field (CEF) effect, such as the case in $CePd_{1-x}Bi_2$.[18] The detailed influence of the CEF effect is out of the scope of the present work, and is subject to further studies, which may provide a fuller understanding of the magnetic ground state of this compound. In the Ce-based heavy fermion materials, where the localized f moments of Ce^{3+} are usually partially screened due to the Kondo coupling, their low-temperature magnetic ground state thus depends on the competition between the Kondo effect and the RKKY interaction.[15,31] In contrast, while the AFM order is driven by the dominating RKKY interaction, no obvious evidence for the Kondo effect can be observed in $PrPd_{0.82}Bi_2$.

3.4. Resistivity

Resistivity ρ vs. T curves of $PrPd_{0.82}Bi_2$ are plotted in Fig. 4. The ρ is almost linear at high temperature above 100 K, which is similar to the behavior of the isostructural $LnNi_{1-x}Sb_2$ (Ln = Tb–Ho)[21] and $CePd_{1-x}Bi_2$,[18] where the Ni or Pd vacancy defects are considered to contribute to the strong scattering. Then ρ is going down gradually with continually decreasing the temperature and then followed by a broad hump at about 60 K, which is possibly consistent with the CEF effect as mentioned in $CeNiX_2$ (X = Si, Ge, Sn)[32] and $CeNiBi_2$.[17] However, no evidence for the Kondo effect, as suggested for $CeTSb_2$ (T = Ni, Cu, Pd, and Ag)[16,33,34] and $CePd_{1-x}Bi_2$,[18] is found in this compound according to the resistivity measurement. As keeping decreasing the temperature, a weak bending feature is observed at 7 K as shown in the upper inset of Fig. 4, associated with the AFM order of the Pr moments, which is in accordance with the behavior in magnetic properties. Moreover, a superconductivity-like behavior appears with an onset temperature of 4 K and a zero-resistivity temperature of 2.7 K without applied magnetic fields, which is likely caused by some minority phases. When increasing the magnetic field, the zero-resistivity behavior is suppressed, which is similar to the case in $LaPd_{0.85}Bi_2$ superconductor.[8]

Specifically, the previous report on the polycrystalline $CeNi_{1-x}Bi_2$ argued that the 6p light electrons of the Bi square-net were responsible for superconductivity,[22] which is quite different from the results obtained on the related single crystals. In $LnNi_{1-x}Bi_2$ (Ln = lanthanide) single crystals, no such bulk superconductivity was detected except in $LaNi_{1-x}Bi_2$, while only Kondo effect and AFM order were observed at low temperature in the rest compounds.[23] However, what happens in $PrPd_{0.82}Bi_2$ single crystals is more similar to that in $CeNi_{1-x}Bi_2$ single crystals.[23] While a small kink in magnetic susceptibility can be noticed at $\sim$ 2.5 K at low magnetic field (see the supplementary information, Fig. S1), no clear experimental signatures for a bulk superconductivity are observed in C_p vs. T and χ vs. T curves. Thus, we argue that some minority phases such as possible superconducting "filament" phase formed in the sample may be responsible for the observed zero-resistivity behavior. Identifying the suspected minority phases could be an interesting topic for further studies of this compound.

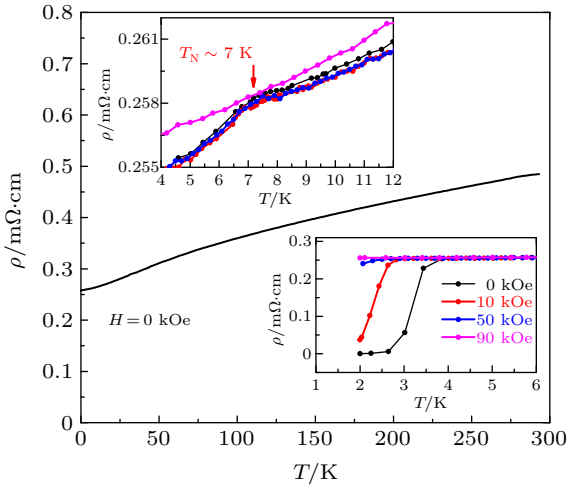


Fig. 4. Resistivity versus temperature plot for $PrPd_{0.82}Bi_2$ without magnetic field. The lower and upper insets are the detailed plots in the regions near T = 2.7 K and T = 7 K, respectively, which is consistent with the onset of zero-resistivity and AFM order, respectively.

3.5. Neutron scattering

Figures 5(a)–5(d) show the polarized neutron diffraction results on single-crystal $PrPd_{0.82}Bi_2$ in the (H 0 L) reciprocal plane for the Xnsf, Xsf, Znsf, and Zsf scattering channels. All of these measurements were performed at 4 K, below the AFM phase transition. According to the separation rule of polarized neutron diffraction on singe crystals, the magnetic scattering contribution appears only in the Xsf channel, and the non-magnetic nuclear coherent scattering contributes only in the Xnsf.[35–38] This provides a simple way to separate magnetic reflections from structural Bragg peaks. As shown in Figs. 5(a) and 5(c), strong magnetic reflections seen in Xsf such as $(-1\ 0\ -2)$ coexist with the nuclear Bragg reflections seen in Xnsf. It can thus be concluded that the propagation wavevector of the low-temperature AFM order is $\boldsymbol{k} = (0\ 0\ 0)$. Furthermore, the absence of any magnetic reflections at $(0\ 0\ L)$ as well as the absence of the magnetic reflections at Znsf such as at $(-1\ 0\ 0)$ would indicate that the magnetic moment of the Pr^{3+} ions should be aligned strictly along the crystallographic c-axis. This is further illustrated in one-dimensional cuts around the $(-1\ 0\ 0)$ reflection for all four measured polarized scattering channels, as shown in Figs. 5(e)–5(f).

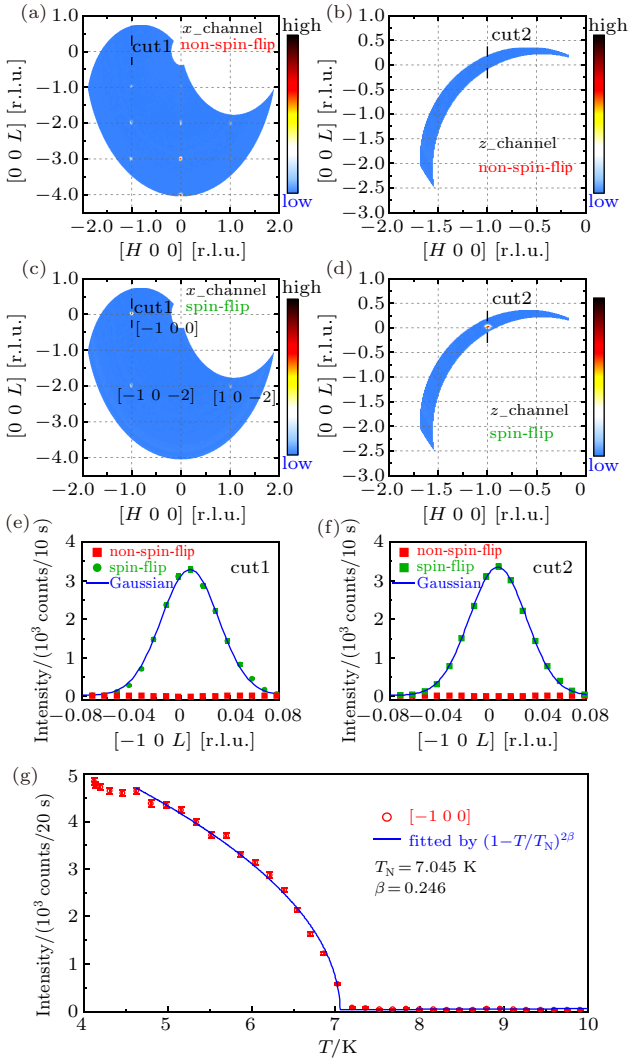


Fig. 5. Contour maps of the polarized neutron diffraction intensities measured on a $PrPd_{0.82}Bi_2$ single crystal in reciprocal space. (a)–(d) Xnsf, Znsf, Xsf, and Zsf scattering in the $(H\,0\,L)$ plane, respectively. (e) and (f) 1D-cuts through the (1 0 0) peak measured in the non-spin-flip (red dot) and spin-flip (green dot) scattering channels, respectively. Note that the measured intensity is too strong to show out the error bar. (g) Temperature dependence of the Xsf scattering intensity of the [1 0 0] peak.

Based on the known space group of the crystalline structure i.e., $P/4nmm$ and the derived magnetic propagation wavevector $\boldsymbol{k} = (0\,0\,0)$, four possible magnetic configurations of the Pr^{3+} moments in the unit cell can be obtained via irreducible representation analysis (see Fig. S2 in the supplementary information). Since the number of the observed magnetic reflections with polarized neutron diffraction is rather limited, nevertheless, our refinements using the obtained single-crystal structure factors clearly indicate that the only possible magnetic structure for $PrPd_{0.82}Bi_2$ is that the c-axis oriented Pr moments form an A-type AFM order, where they are ferromagnetically coupled in the ab-plane, but antiferromagnetically coupled between the neighboring planes, as shown in Fig. 7. The single-crystal refinement yields an ordered magnetic moment of $\mu_{\rm eff} \approx 2.38\ \mu_{\rm B}$, which is smaller than the effective moment of free Pr^{3+} ions. However, as we could only detect a few magnetic diffraction peaks in this instrument, the refined result from single crystals probably has a large error in contrast to the result refined from powder samples that we will discuss below.

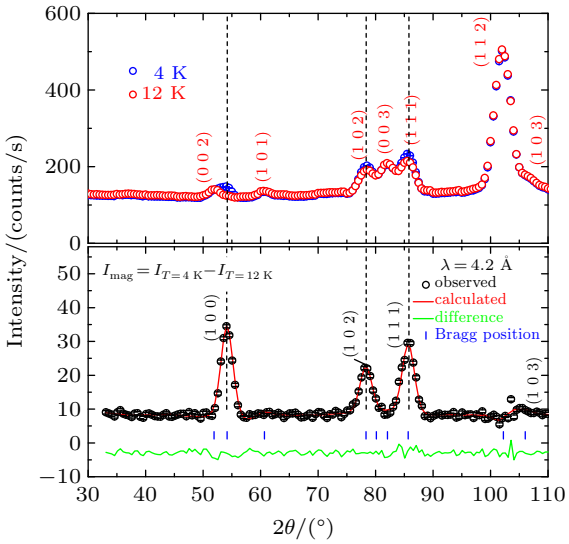


Fig. 6. Powder neutron diffraction patterns measured with the non-polarized setup at DNS, the neutron wavelength is 4.2 Å. (a) Data taken at $T = 4$ K and 12 K, respectively. The nuclear peaks are indexed as red indices. (b) The intensity difference pattern between 4 K and 12 K as well as the Rietveld refinement of the magnetic intensities by using the Fullprof software. The magnetic peaks are shown as black indices.

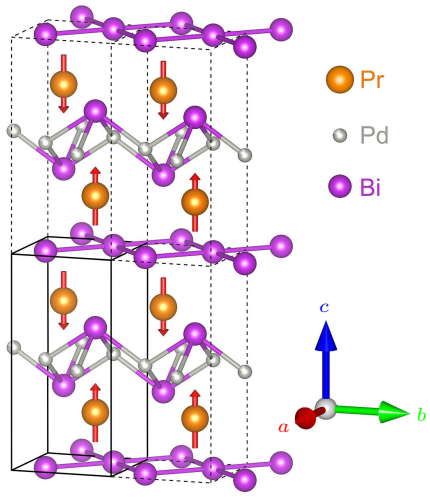


Fig. 7. Schematic view of the combined crystalline and magnetic structure of $PrPd_{0.82}Bi_2$.

The temperature dependence of the Xsf scattering intensity of the magnetic peak [1 0 0], as shown in Fig. 5(g), clearly indicates a second-order magnetic phase transition at $T_{\rm N} \sim 7$ K. The data near the critical point can be fitted by using a spontaneous magnetization model with the following formula:

$$I = I_0 \left(1 - \frac{T}{T_{\rm N}}\right)^{2\beta}, \quad (T < T_{\rm N}),$$

where I is the measured scattering intensity, $T_{\rm N}$ is the phase transition temperature, and β is the critical exponent.[39,40]

The value of β is usually used to determine the type of magnetic models of the spontaneous magnetization. For the two-dimensional (2D) Ising model, $\beta = 0.125$; for three-dimensional (3D) Ising model, $\beta = 0.326$; for 3D Heisenberg model, $\beta = 0.367$. The data below T_N was well fitted by this formula, yielding $T_N = 7.04$ K and $\beta = 0.24$, which indicates that $PrPd_{0.82}Bi_2$ can be classified as a quasi-2D Ising system.

In order to determine the ordered magnetic moment precisely, additional non-polarized NPD experiment was performed on a $PrPd_{0.82}Bi_2$ powder sample that was grounded from a small single crystal. As plotted in Fig. 6(a), the diffraction intensities measured at $T = 12$ K (named as $I_{T=12\ K}$) are pure nuclear coherent scattering signals due to the crystalline structure, while the data collected at $T = 4$ K (named as $I_{T=4\ K}$) are the combined nuclear coherent and magnetic scattering contributions. Besides, no structural phase transition was observed in $PrPd_{0.82}Bi_2$ as well as in the other 112-type family of materials. The magnetic contribution can be obtained by subtracting the nuclear scattering contributions measured at $T = 12$ K from the data $I_{T=4\ K}$.[19,41,42] As shown in Fig. 6(b), a number of magnetic peaks are clearly observed after subtraction. The Rietveld refinement of the magnetic structure was undertaken by using the FullProf software, revealing a good agreement between the observed and calculated intensities with R factors being $R_p = 5.61\%$, $R_w = 7.74\%$, $\chi^2 = 2.82$. Meanwhile, the refined ordered magnetic moment of the Pr ions is 1.694(3) μ_B, which is much smaller than 3.58 μ_B for effect moments of free Pr^{3+} ions. One of the possible reasons for the reduced ordered magnetic moments may be due to the incompletely saturated moment at 4 K, which is the lowest temperature reached in our neutron diffraction experiments. Moreover, the CEF effect and possible Kondo effect, usually presented in the 112-type materials,[17,18,20] may also contribute to the reduction of the magnetic moment in $PrPd_{0.82}Bi_2$.

4. Conclusion

$PrPd_{0.82}Bi_2$ single crystals were successfully grown and their physical properties, including heat capacity, magnetic properties, and resistivity, as well as the low-temperature magnetic structure were studied by complementary in-house characterization and neutron powder and single-crystal diffraction. We found that $PrPd_{0.82}Bi_2$ shows an AFM phase transition with $T_N \sim 7$ K. Meanwhile, a spin-flop transition occurs as increasing the applied magnetic field at 2 K. A large Sommerfeld coefficient, reaching to 329.23 $mJ \cdot mol^{-1} \cdot K^{-2}$, suggests a heavy-fermion like behavior that may be due to the interaction between the localized 4f electrons of Pr^{3+} ions and itinerant charge carriers. Furthermore, the resistivity reaches to zero at ~ 2.7 but no obvious diamagnetic behavior is detected, implying that it may be not a bulk superconductor but caused by minority phases. Neutron scattering experiments performed on both single crystals and grinding powders reveal an A-type AFM order of Pr^{3+} ions below T_N. The magnetic moments of Pr^{3+} ions are strictly aligned along the crystallographic c-axis, behaving like a quasi-2D Ising spin system. The ordered magnetic moment refined from neutron powder diffraction data is estimated to be 1.694(3) μ_B, which is smaller than that of a free Pr^{3+} ion. Further studies may be needed to clarify such as the origin of superconductivity, the influence of the CEF effect on the magnetic ground state of Pr^{3+} ions, and possible heavy fermion behavior in this layered antiferromagnet $PrPd_{0.82}Bi_2$.

References

[1] Kamihara Y, Watanabe T, Hirano M and Hosono H 2008 *J. Am. Chem. Soc.* **130** 3296
[2] Matsuishi S, Inoue Y, Nomura T, Yanagi H, Hirano M and Hosono H 2008 *J. Am. Chem. Soc.* **130** 14428
[3] Rotter M, Tegel M and Johrendt D 2008 *Phys. Rev. Lett.* **101** 107006
[4] Wang X C, Liu Q Q, Lv Y X, Gao W B, Yang L X, Yu R C, Li F Y and Jin C Q 2008 *Solid State Commun.* **148** 538
[5] Johnston D C 2010 *Adv. Phys.* **59** 803
[6] Ding H, Richard P, Nakayama K, Sugawara K, Arakane T, Sekiba Y, Takayama A, Souma S, Sato T, Takahashi T, Wang Z, Dai X, Fang Z, Chen G F, Luo J L and Wang N L 2008 *Europhys. Lett.* **83** 47001
[7] Kurian J, Buckow A, Retzlaff R and Alff L 2013 *Physica C* **484** 171
[8] Han F, Malliakas C D, Stoumpos C C, Sturza M, Claus H, Chung D Y and Kanatzidis M G 2013 *Phys. Rev. B* **88** 144511
[9] Retzlaff R, Buckow A, Komissinskiy P, Ray S, Schmidt S, Mühlig H, Schmidl F, Seidel P, Kurian J and Alff L 2015 *Phys. Rev. B* **91** 104519
[10] Katayama N, Kudo K, Onari S, Mizukami T, Sugawara K, Sugiyama Y, Kitahama Y, Iba K, Fujimura K, Nishimoto N, Nohara M and Sawa H 2013 *J. Phys. Soc. Jpn.* **82** 123702
[11] Yakita H, Ogino H, Okada T, Yamamoto A, Kishio K, Tohei T, Ikuhara Y, Gotoh Y, Fujihisa H, Kataoka K, Eisaki H and Shimoyama J 2014 *J. Am. Chem. Soc.* **136** 846
[12] Park J, Lee G, Wolff-Fabris F, Koh Y Y, Eom M J, Kim Y K, Farhan M A, Jo Y J, Kim C, Shim J H and Kim J S 2011 *Phys. Rev. Lett.* **107** 126402
[13] Huang S, Kim J, Shelton W A, Plummer E W and Jin R 2017 *Proc. Natl. Acad. Sci. USA* **114** 6256
[14] Wang Y Y , Yu Q H and Xia T L 2016 *Chin. Phys. B* **25** 107503
[15] Gignoux D and Gomez-Sal J 1984 *Phys. Rev. B* **30** 3967
[16] Muro Y, Takeda N and Ishikawa M 1997 *J. Alloys Compd.* **257** 23
[17] Jung M H, Lacerda A H and Takabatake T 2002 *Phys. Rev. B* **65** 132405
[18] Han F, Wan X, Phelan D, Stoumpos C C, Sturza M, Malliakas C D, Li Q, Han T H , Zhao Q, Chung D Y and Kanatzidis M G 2015 *Phys. Rev. B* **92** 045112
[19] Kolenda M, Hofmann M, Leciejewicz J, Penc B, Szytula A and Zygmunt A 2001 *J. Alloys Compd.* **315** 22
[20] Seibel E M, Xie W, Gibson Q D and Cava R J 2015 *J. Solid State Chem.* **230** 318
[21] Thomas E L, Moldovan M, Young D P and Chan J Y 2005 *Chem. Mater.* **17** 5810
[22] Mizoguchi H, Matsuishi S, Hirano M, Tachibana M, Takayama-Muromachi E, Kawaji H and Hosono H 2011 *Phys. Rev. Lett.* **106** 057002
[23] Lin X, Straszheim W E, Bud'ko S L and Canfield P C 2013 *J. Alloys Compd.* **554** 304
[24] Farhan M A, Lee G and Shim J H 2014 *J. Phys.: Condens. Matter* **26** 042201
[25] Masuda H, Sakai H, Tokunaga M, Yamasaki Y, Miyake A, Shiogai J, Nakamura S, Awaji S, Tsukazaki A, Nakao H, Murakami Y, Arima T, Tokura Y and Ishiwata S 2016 *Sci. Adv.* **2** e1501117

[26] Kealhofer R, Jang S, Griffin S M, John C, Benavides K A, Doyle S, Helm T, Moll P J W, Neaton J B, Chan J Y, Denlinger J D and Analytis J G 2018 *Phys. Rev. B* **97** 045109
[27] Borisenko S, Evtushinsky D, Gibson Q, Yaresko A, Koepernik K, Kim T, Ali M, van den Brink J, Hoesch M, Fedorov A, Haubold E, Kushnirenko Y, Soldatov I, Schäfer R and Cava R J 2019 *Nat. Commun.* **10** 3424
[28] Liu J Y, Hu J, Zhang Q, Graf D, Cao H B, Radmanesh S M A, Adams D J, Zhu Y L, Cheng G F, Liu X, Phelan W A, Wei J, Jaime M, Balakirev F, Tennant D A, DiTusa J F, Chiorescu I, Spinu L and Mao Z Q 2017 *Nat. Mater* **16** 905
[29] Yi C, Yang S, Yang M, Wang L, Matsushita Y, Miao S, Jiao Y, Cheng J, Li Y, Yamaura K, Shi Y and Luo J 2017 *Phys. Rev. B* **96** 205103
[30] Wang H P, Wu D S, Shi Y G and Wang N L 2016 *Phys. Rev. B* **94** 045112
[31] Beyermann W P, Hundley M F, Canfield P C, Thompson J D, Latroche M, Godart C, Selsane M, Fisk Z and Smith J L 1991 *Phys. Rev. B* **43** 13130
[32] Pecharsky V, Gschneidner Jr K and Miller L 1991 *Phys. Rev. B* **43** 10906
[33] Sologub O, Hiebl K, Rogl P, Noël H and Bodak O 1994 *J. Alloys Compd.* **210** 153
[34] Thamizhavel A, Takeuchi T, Okubo T, Yamada M, Asai R, Kirita S, Galatanu A, Yamamoto E, Ebihara T, Inada Y, Settai R and Ōnuki Y 2003 *Phys. Rev. B* **68** 054427
[35] Moon R M, Riste T and Koehler W C 1969 *Phys. Rev.* **181** 920
[36] Rodríguez-Carvajal J 1993 *Physica B* **192** 55
[37] Ressouche E 2014 ed V Simonet B Canals J. Robert S Petit and H Mutka *JDN* **13** 02001
[38] Schärpf O and Capellmann H 1993 *Phys. Stat. Sol. (a)* **135** 359
[39] Blundell S 2014 *Magnetism in Condensed Matter* (Oxford: Oxford Univ. Press)
[40] Pelissetto A and Vicari E 2002 *Phys. Rep.* **368** 549
[41] Kodama K, Wakimoto S, Igawa N, Shamoto S, Mizoguchi H and Hosono H 2011 *Phys. Rev. B* **83** 214512
[42] Adriano C, Rosa P F S, Jesus C B R, Mardegan J R L, Garitezi T M, Grant T, Fisk Z, Garcia D J, Reyes A P, Kuhns P L, Urbano R R, Giles C and Pagliuso P G 2014 *Phys. Rev. B* **90** 235120